



# **Correlative imaging of biological cells using simultaneous ptychography and X-ray fluorescence**

Dorota Puzio

AGH University of Science and Technology, Poland

Supervisor: Karolina Stachnik

September 6, 2017

## **ABSTRACT**

The following report presents my work during the DESY Summer Student Programme 2017 in Hamburg. I was assigned to Photon Science group and working on correlative imaging of biological cells using simultaneous ptychography and X-ray fluorescence.

This report shall give an overview of combining both methods and possibilities of using in bioimaging for qualitative and quantitative study of biological samples. Macrophages infected with tuberculosis were examined. The experimental part, carried out at beamline P11 of PETRA III, is described, data processing and results are discussed.

# LIST OF CONTENTS

<b>1. Introduction</b>	<b>3</b>
1.1 Ptychography	3
1.2 X-ray Fluorescence	4
<b>2. Tuberculosis</b>	<b>4</b>
2.1 Mechanism of TB therapy	5
<b>3. Experimental part</b>	<b>6</b>
3.1 Sample preparations	6
3.2 Experimental setup	6
<b>3.3 Data analysis</b>	<b>8</b>
3.3.1 Calibration of incoming intensity measurement	8
3.3.2 XRF spectra fitting	9
3.3.3 Ptychographic reconstruction	10
3.3.4 Overlaying XRF map onto ptychographic phase image	11
3.3.4 Calibration of Fe surface mass using XRF standard	11
<b>4. Conclusions</b>	<b>13</b>
<b>References</b>	<b>14</b>

# 1. Introduction

Studies of cells and tissues often require multiple imaging methods be employed. Thanks to high spatial coherence of the beam and high flux provided by the third-generation synchrotron radiation sources, and advanced instrumentation, it has become possible to simultaneously measure specimen's structure (X-ray ptychographic CDI) and function (XRF). Here, the combination of X-ray fluorescence and ptychography for imaging biological cells is demonstrated. This combined approach has significant impact on studies of the intracellular localisation of nanocomposites with attached therapeutic or diagnostic agents, and helps to clarify the roles of trace metals in cell development.

Coherent Diffractive Imaging (CDI) uses a coherent X-ray beam to illuminate a sample and retrieves the phase information on the sample from phase-retrieval analysis of the far-field diffraction pattern. From the many CDI variants developed, ptychography has been shown to be the most robust, being a scanning technique where coherent diffraction information is collected from overlapping regions and used to reconstruct the sample complex optical density properties.

Moreover, ptychography offers a path to imaging biological structure at beyond-focusing-optic resolution, while X-ray fluorescence microscopy provides sensitivity for quantitative mapping of elements, especially trace metals, which play a crucial role in many biological processes.

## 1.1 Ptychography

Ptychography is a high resolution, scanning-based coherent diffractive imaging (CDI) technique. The sample is illuminated with a focused, coherent (laser-like) X-ray beam and small angle scattering patterns are collected as the sample is raster scanned through the beam. The scattering patterns and the precise beam positions on the sample are fed into a Fourier transform-based, iterative algorithm which returns a real-space image that contains both the phase and absorption information of the sample. The resulting image has a resolution better than the size of the focused X-ray beam. Therefore, the resolution of the technique is not limited by the size of the focused beam footprint on the sample, which allows imaging below the current resolution limits of the most state-of-the-art X-ray optics. Ptychography does not require a crystalline sample as with standard X-ray diffraction nor an isolated sample as with standard, full-field CDI [1].

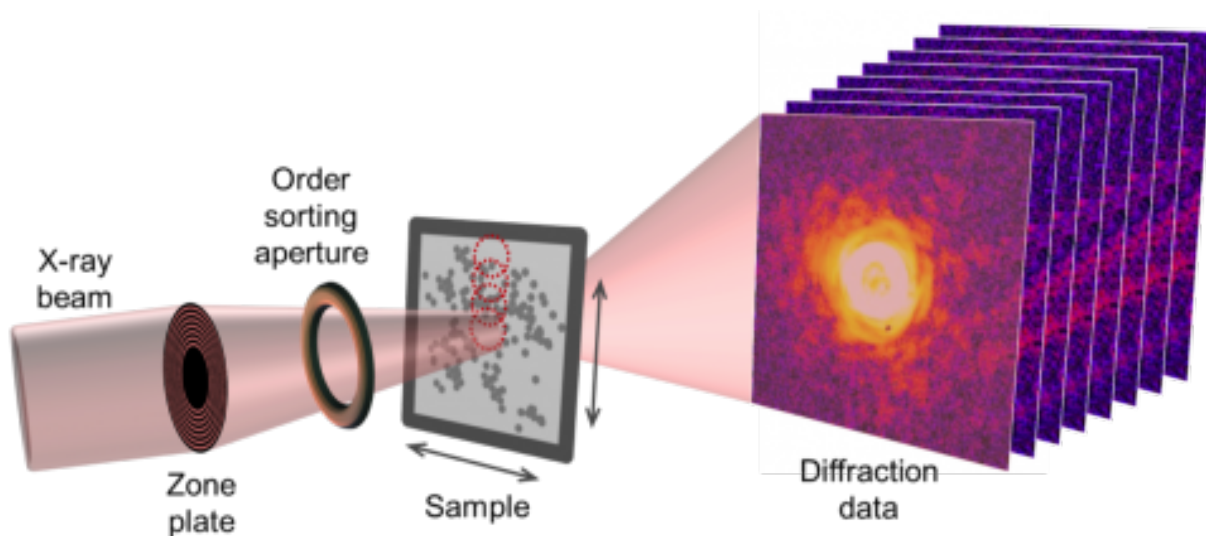


Fig.1. Simplified scheme of ptychographic setup [2].

## 1.2 X-ray Fluorescence

When an incoming X-ray photon is absorbed, it will knock-out an electron from one of absorbing atom's orbitals, provided that its energy is larger than the binding energy of the corresponding electron.

The atom with this vacancy will relax back into its ground state through transition of an electron from a higher orbital into the vacant state following one of two possible processes: fluorescence - the energy is released in form of a photon of the corresponding energy difference, or Auger process - the energy is transferred to another electron from one of the outer shells, which is ejected from the atom as Auger electron.

The probability that the relaxation occurs through the process of fluorescence is low for low-Z elements and high for high-Z elements. Hence, making fluorescence detection from biological matters which mainly constitute of light elements (carbon, nitrogen, oxygen) is rather challenging [1].

## 2. Tuberculosis

Tuberculosis (TB) according to the World Health Organisation (WHO) is one of the most prevalent infectious disease worldwide causing high mortality. TB has regained tremendous



attention owing to its deadly liaison with HIV as well as due to the alarming emergence of multidrug resistant and extremely drug resistant isolates.

Notably, about one third of the world's population is estimated to be latently infected, with a 10% chance to become active during life time. The pathogenic agent, *Mycobacterium tuberculosis* (*M.tb.*), resides as facultative intracellular parasite in macrophages encapsulated in granulomas. Therefore, therapy, especially of latent TB, remains a big challenge [3].

## 2.1 Mechanism of TB therapy

Due to *M.tb.* properties, anti-mycobacterial drugs have not only to cross the granuloma encapsulation and the host macrophage membrane but also the lipid-rich cell wall of the mycobacterial cell. Additional restrictions are related to the limited permeability into biofilms and their rapid degradation in the physiological environment at low dose, but heavy side-effects at higher doses.

Hence, nanomaterials seem to be promising for tuberculosis therapy - efficient shuttle systems to infiltrate infected cells with antibiotics are highly desired. Requirements set for this type of shuttle are large capacity of antibiotics, biocompatibility, biodegradability and optimal time of excreting residue-free.

In this case, a new strategy of using isoniazid-filled iron oxide nanocontainers (INH@Fe<sub>2</sub>O<sub>3</sub>) for tuberculosis therapy is examined. The nanocontainers have a uniform, spherical morphology with an outer diameter of 15-20 nm, a wall thickness of 2-4 nm, and an inner cavity diameter of 8-10 nm. The load of the nanocontainers was quantified by different methods. Thus, the nanocontainers consisted of 9 wt% of water, 48 wt% of isoniazid (INH) in the inner cavity, and 43 wt% Fe<sub>2</sub>O<sub>3</sub> as the sphere wall. At about half of the total weight, INH-load is significantly higher in comparison to known nanoparticles [4]. To improve membrane permeability and cell uptake, nanocontainers were functionalized with dextran (DEX).

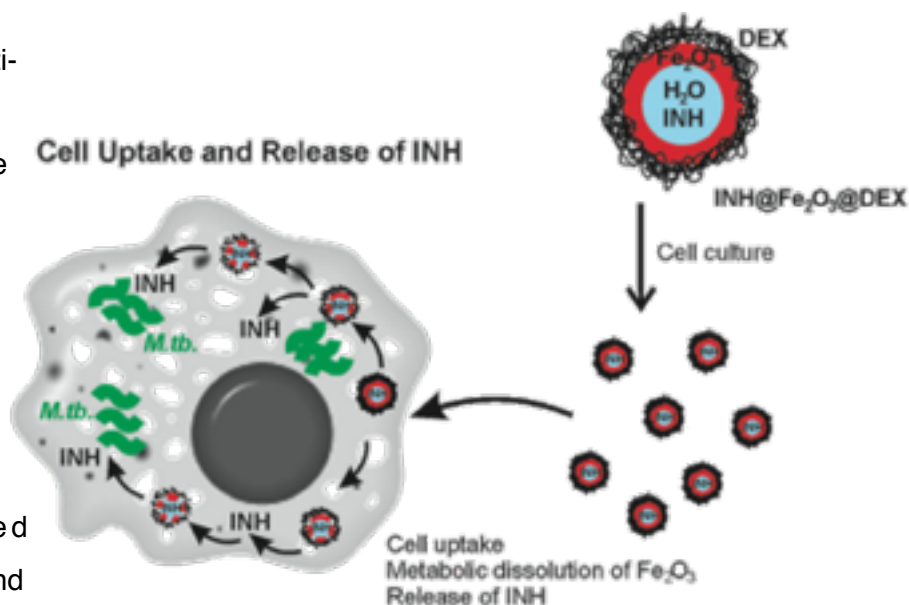


Fig.2. Schematic view of TB therapy's mechanism[4].

Schematic view of INH@Fe<sub>2</sub>O<sub>3</sub>@DEX nanocontainers uptake and INH-release in *M.tb.*-infected macrophages is shown in Fig.2. The nanocontainers are actively internalized into macrophages. As iron is an essential nutrient for growth and virulence, the nanocontainers can be considered as “Trojan horses” for antibiotics. They release INH inclose proximity to the mycobacteria upon slow metabolic dissolution of the Fe<sub>2</sub>O<sub>3</sub> wall, exploiting the mycobacterial’s need for iron.

### 3. Experimental part

#### 3.1 Sample preparations

Bone marrow derived macrophages infected with *M.tb.* and treated with Fe-nanoclusters were examined. Before the experiment, preselection of cells with visible light microscopy had been done. Region of interest was marked with yellow rectangle, bacterias were labelled with fluorescent protein marker (Fig.3,4).

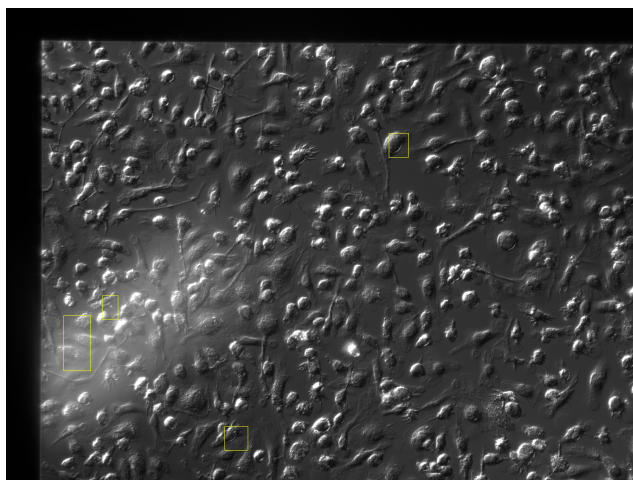


Fig.3. Differential interference contrast

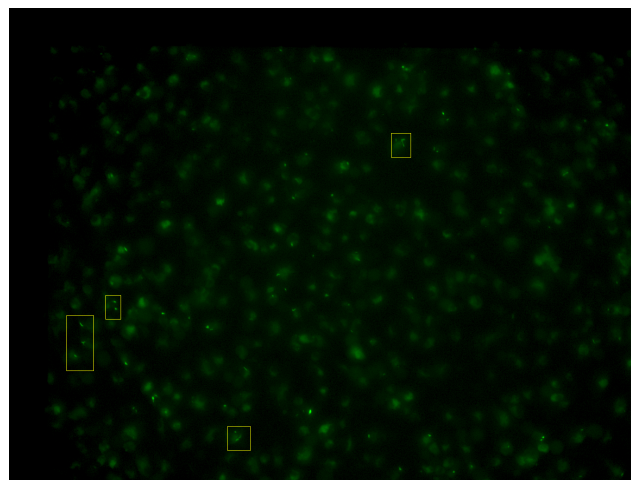


Fig.4. Visible light fluorescence

#### 3.2 Experimental setup

The experiment was carried out at beamline P11 at the PETRA III synchrotron light source. A well-defined and collimated undulator beam at a photon energy of 7.4 keV was used. The coherent portion of the beam was formed using beam defining slits set to 40 um in horizontal plane and 60 um in vertical plane. Coherent X-ray wavefront was produced by a partially

illuminated (off-axis) focusing Fresnel zone plate (FZP), mounted upstream of the order sorting aperture (OSA) of a diameter of  $10\text{ }\mu\text{m}$ . The schematic view is shown in Fig.5.

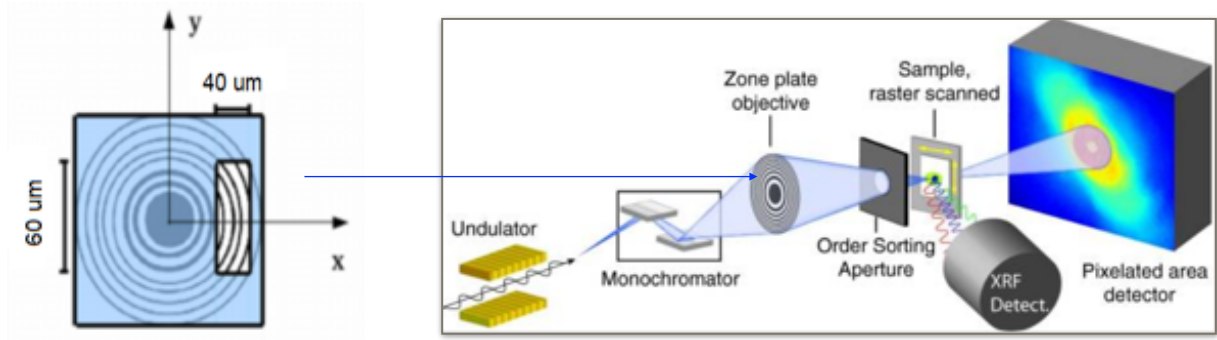


Fig.5. Schematic view of experimental setup for simultaneous ptychographic and X-ray fluorescence imaging with off-axis focusing FZP taken into account [5].

To carry out experiment which combines both methods, the special geometry of experimental setup is crucial. A silicon drift X-ray detector (Vortex EM) was mounted at  $56^\circ$  with regard to the incident X-ray beam to collect fluorescence signal (Fig.6). A Dectris Pilatus 1M single-photon-counting hybrid pixel array detector was positioned 4.2 m behind the sample to record diffraction patterns. To reduce the time overhead caused by standard step-scan approach, continues-motion-scan (fly-scan) along the horizontal axis with carriage return was implemented. The sample's positions were monitored by laser interferometers. Experiment was conducted with a scanning step size of  $80\text{ nm}$ , an exposure time  $100\text{ ms}$  and fly-scan velocity  $0.8\text{ }\mu\text{m/s}$ .

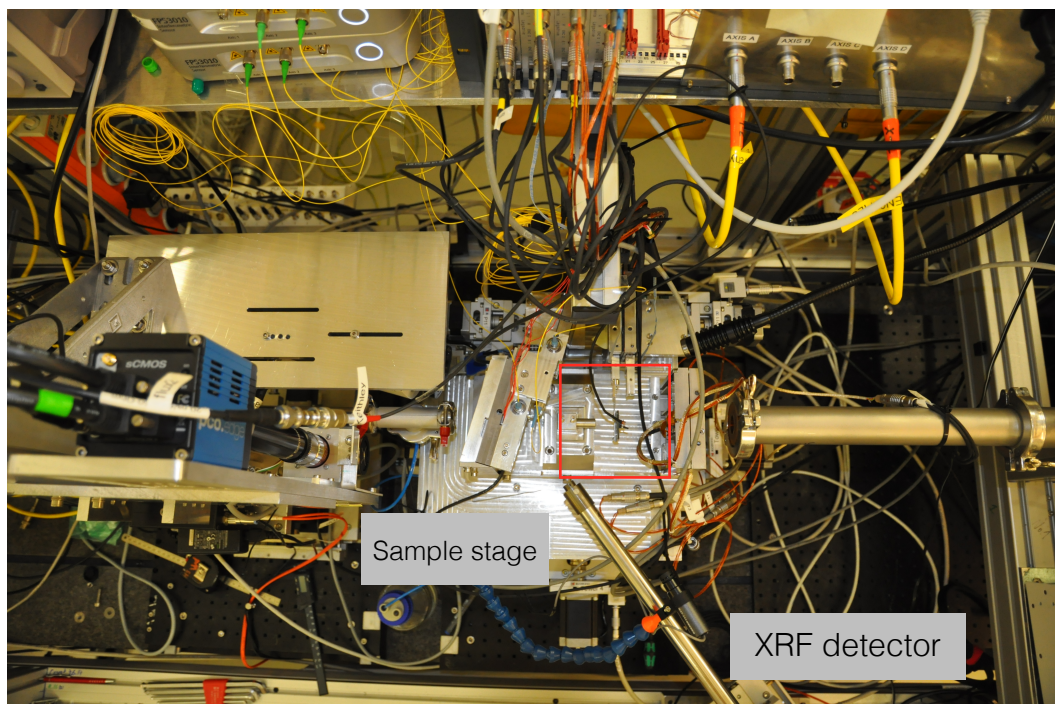


Fig.6. Beamline P11 ptychography and X-ray fluorescence setup (probe defining instruments marked in red).

### 3.3 Data analysis

For reconstructions of ptychographic datasets the difference map algorithm was implemented [6]. Then, some improvements were necessary. Due to fluctuations of the beam, a diode measuring the incoming intensity was installed. Therefore, there was a possibility to normalize data sets using the diode signal.

#### 3.3.1 Calibration of incoming intensity measurement

To normalise diode readout, all values were divided by maximum value, then calibration was used to obtain values oscillating around 1. After that, the raw image was divided by the normalized diode readout. Normalisation was tested on transmission images from STXM (scanning transmission X-ray microscopy). Fig. 7-10 depict normalisation step-by-step.

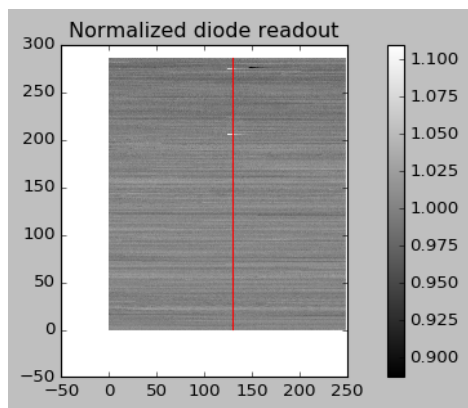


Fig.7. Normalized diode readout

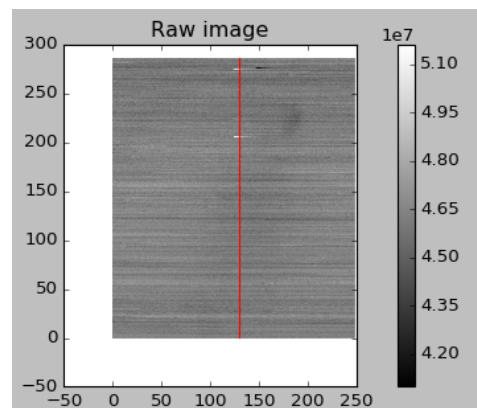
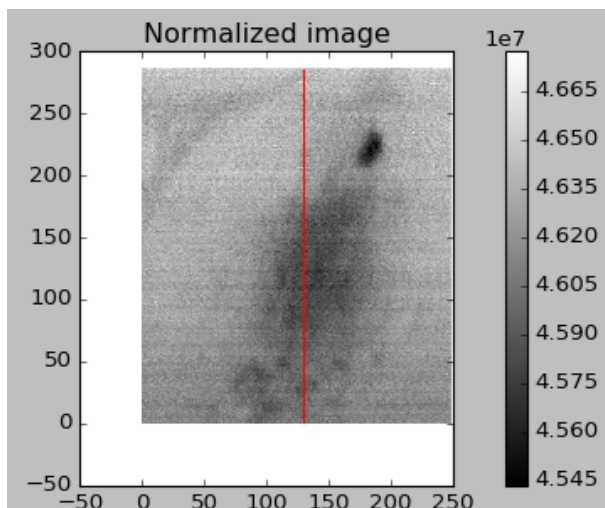


Fig.8. Raw transmission STXM image (colorbar shows photon counts).



Fig.9 Line plot (marked in red in Figs. 7,8,10) through the diode readout, raw image and normalized image.





One can easily see that the raw image is noisy and it is impossible to distinguish a cell in it. The normalized image, thanks to correction with for changes in incoming intensity, has correct contrast. Normalization lets images be independent of fluctuation of incoming.

Fig.10. Resulting, normalized image.

### 3.3.2 XRF spectra fitting

For XRF spectra interpretation PyMca was used. It lets identify individual elemental contributions to complicated spectra and makes a good estimation of the concentrations of the elements. An exemplary cumulative spectrum is shown in Fig.11.

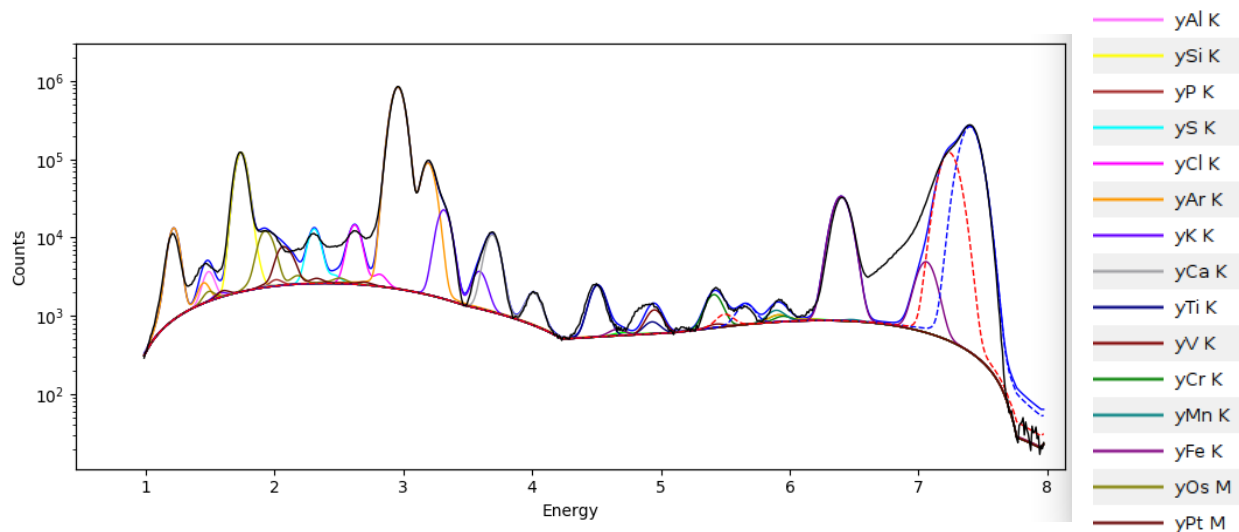


Fig.11. Cumulative spectrum of XRF fluorescence signal from cell.

As describe in subchapter 3.3.1, the PyMca-fitted XRF elemental maps have been normalized with incoming intensity photon flux, to obtain independence from fluctuation.

### 3.3.3 Ptychographic reconstruction

Ptychographic reconstruction was done with 3 illumination modes, using 200 iteration. To resolve problem with phase gradient some correction was necessary. Firstly, polynomial of third order was fitted, to correct main trend. Then, to get better result polynomial of 9th order was fitted. Fig.12 depicted phase gradient correction procedure step-by-step.

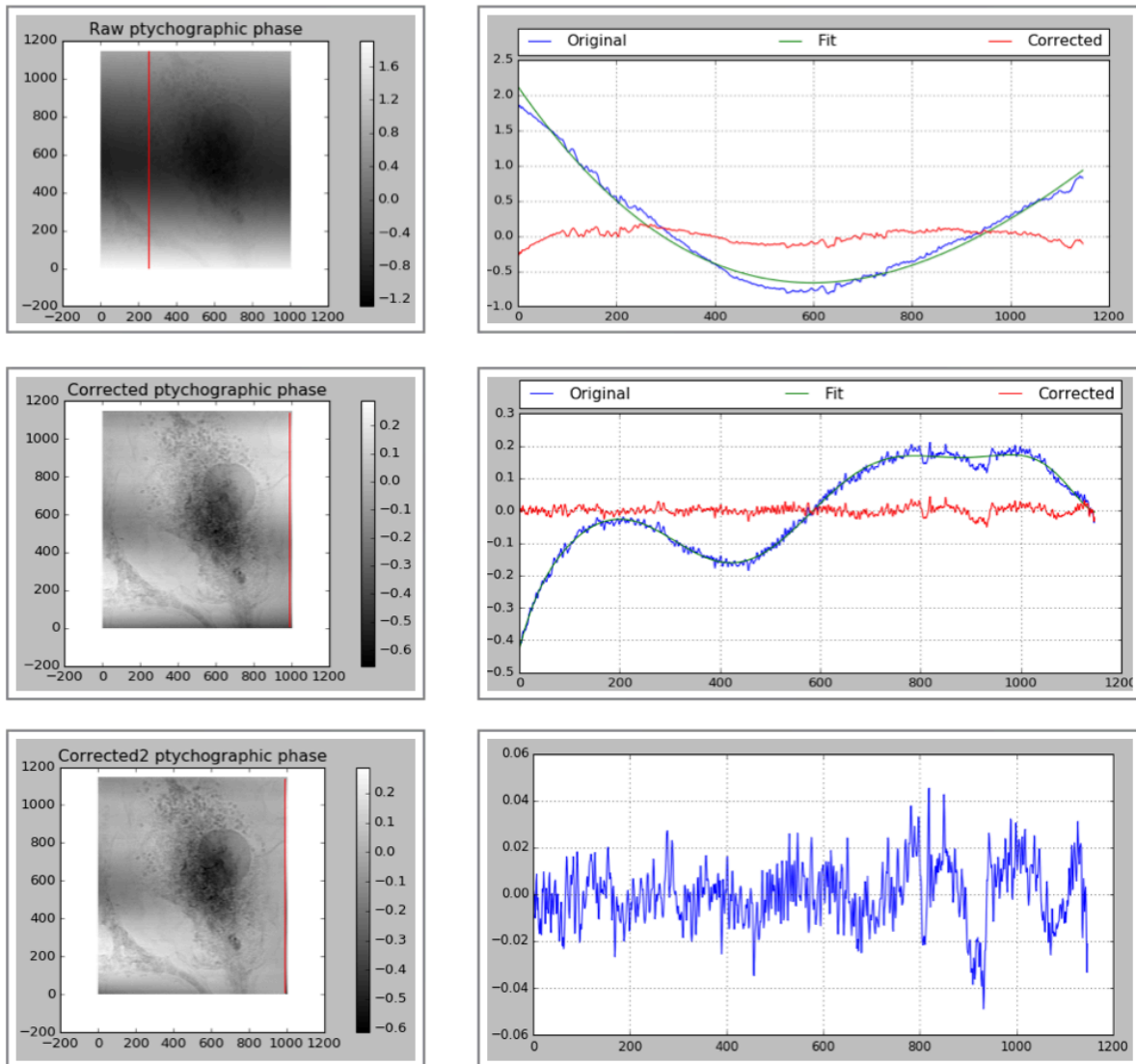


Fig.12. Results of phase offset's correction (colorbars show phase shift in radians).

One can see that original phase stays within range from -1.0 to 2.0 radians. After correction, the resulting image phase significantly improves, corrected phase in the region without sample ranges between -0.04 and 0.04 radians.

### 3.3.4 Overlaying XRF map onto ptychographic phase image

Having a well-prepared reconstruction, and normalised XRF images, overlaying is possible. Due to difference in sizes, STXM images were used as tool to align XRF maps. Since they have the same sizes and also present a biological structure, it is much easier to precisely overlay images. XRF images were properly cropped and overlaid on ptychographic reconstruction. The results were shown in Fig.13.

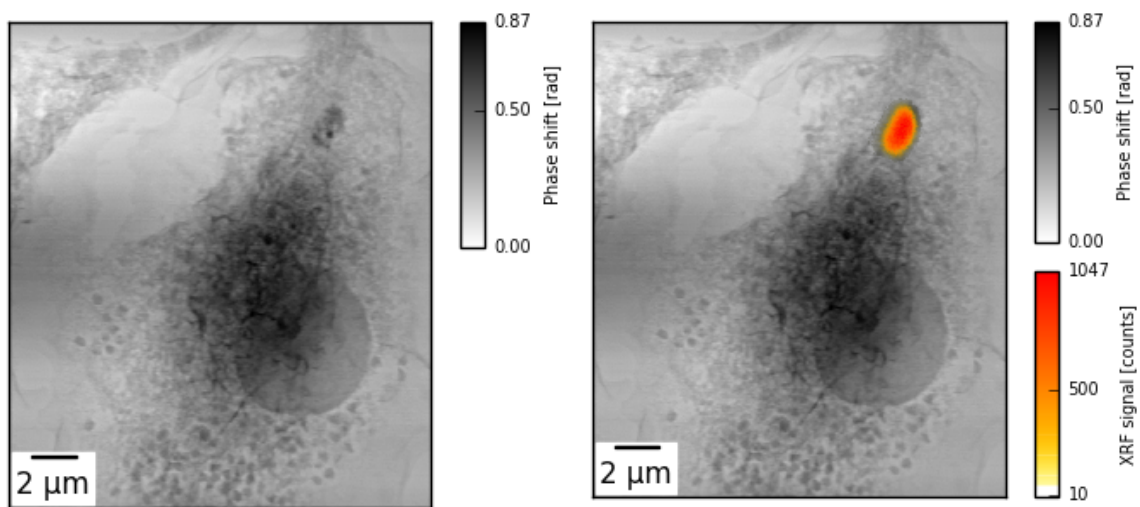


Fig.13. Ptychographic reconstruction and XRF image overlaid onto ptychographic reconstruction.

### 3.3.4 Calibration of Fe surface mass using XRF standard

To have a possibility to calibrate Fe surface mass, XRF standard (Fe layer with a thickness of 470 nm) was scanned. Then, fitted Fe map was normalized with incoming intensity. Assuming homogeneity of the Fe layer, what is shown in Fig. 14, the average value of counts was taken to calibration.

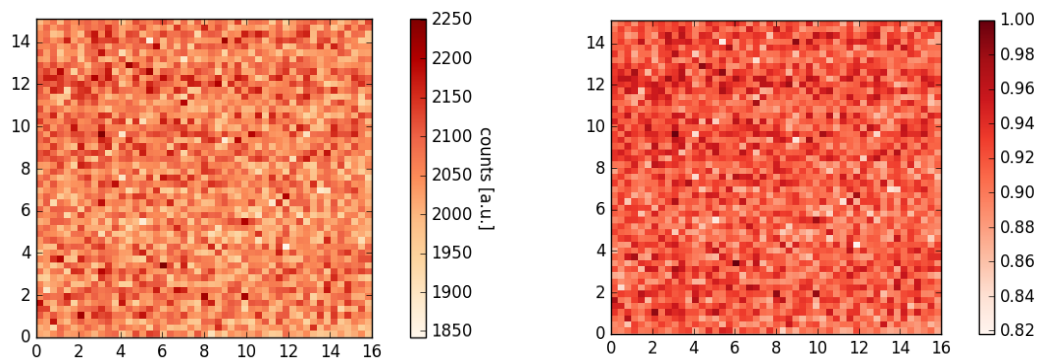


Fig.14. Fe K-line map of Fe XRF calibration standard: left image - signal in counts, right image:

Histogram of all pixel values was plotted. Then Gaussian curve was fitted. The mean value is 2057.6 counts and with variance 55.8 counts.

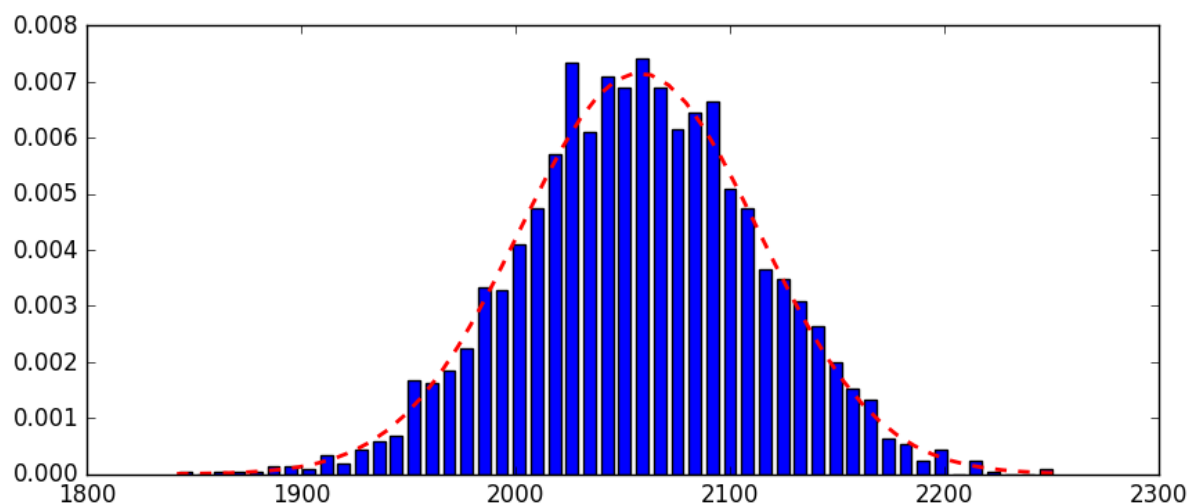


Fig.12 Histogram of Fe counts with Gaussian fit.

Then, having the calibration, Fe map of measured cell was recalculated from counts to surface mass.

Fe density:  $7,874 \text{ g/cm}^3 = 7874 \text{ ug/mm}^3$

Fe layer thickness: 470 nm

Fe layer effective thickness (taking account tilted sample stage) = 487 nm

Surface mass:  $3,83 \text{ ug/mm}^2$

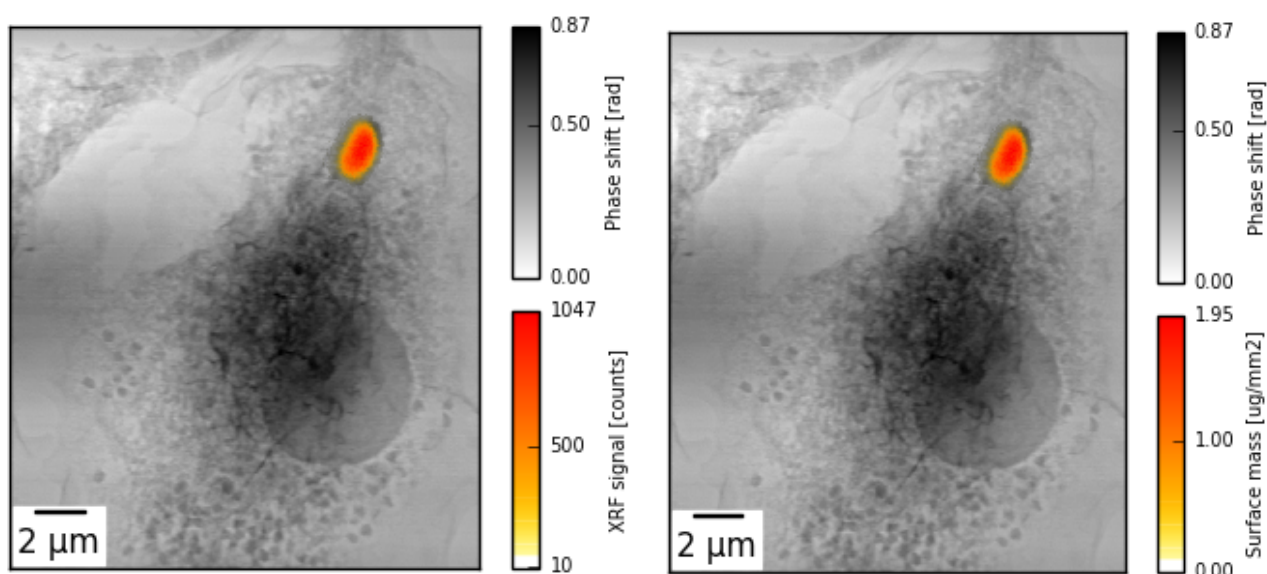


Fig.13 Fe map overlaid onto ptychographic reconstruction: the left one - XRF signal in counts, the right one - XRF counts calculated to surface mass.



## 4. Conclusions

The ptychographical coherent X-ray diffractive imaging is a powerful and promising method yielding almost diffraction-limited resolution with no use of any lenses or optical components. In combination with nanoscale X-ray fluorescence is a great tool, which gives information about intracellular localisation of nanoparticles with attached therapeutic or diagnostic agent. Hence, this combined approach will have significant impact on developing new strategy for different disease's therapies.

My project allowed me to study the theoretical background of ptychography, get familiarised with experimental technique, learn data analysis and finally, participate in an experiment at beamline P11.

# References

- [1] J. Als-Nielsen, D. McMorrow, Elements of modern X-ray physics; 2nd ed., Wiley, Hoboken, NJ, 2011.
- [2] <https://www-ssrl.slac.stanford.edu/wekergroup/ptychography>.
- [3] [http://www.who.int/tb/publications/global\\_report/en/](http://www.who.int/tb/publications/global_report/en/)
- [4] P. Leidinger, et al., Angew. Chem. Int. Edit. 54 (2015) 12597–12601.
- [5] J. Deng, et al., Proc. Natl. Acad. Sci. U. S. A., 112 (2015), 2314–2319.
- [6] P. Thibault, et al., Ultramicroscopy 190(2009) 338-343.